Pan et al. *Zool. Res.* 2025, 46(5): 953−966
https://doi.org/10.24272/j.issn.2095-8137.2024.475
https://cstr.cn/32248.14.zr.2024.475

ZR | Zoological Research

Article Open Access

Single-cell atlas of grass carp (*Ctenopharyngodon idella*) peripheral blood IgM$^+$ B cells provides insights into B cell-mediated immune responses in teleost fish

Yi-Ru Pan[1], Xue-Qing Han[1], Tian-Tian Tian[1], Yong-An Zhang[1,2,3,*], Xu-Jie Zhang[1,2,3,*]

[1] *National Key Laboratory of Agricultural Microbiology*, *Hubei Hongshan Laboratory*, *Engineering Research Center of Green Development for Conventional Aquatic Biological Industry in the Yangtze River Economic Belt*, *Ministry of Education*, *College of Fisheries*, *Huazhong Agricultural University*, *Wuhan*, *Hubei* 430070, *China*

[2] *Shenzhen Institute of Nutrition and Health*, *Huazhong Agricultural University*, *Wuhan*, *Hubei* 430070, *China*

[3] *Shenzhen Branch*, *Guangdong Laboratory for Lingnan Modern Agriculture*, *Genome Analysis Laboratory of the Ministry of Agriculture*, *Agricultural Genomics Institute at Shenzhen*, *Chinese Academy of Agricultural Sciences*, *Shenzhen*, *Guangdong* 518124, *China*

ABSTRACT

Teleost peripheral blood contains a remarkably high proportion of B cells, accounting for 15%–50% of circulating lymphocytes. However, their immune responses to bacterial infection are yet to be elucidated. In the present study, 10× Genomics single-cell RNA sequencing (scRNA-seq) was employed to characterize the transcriptomic landscape of peripheral blood IgM$^+$ B cells in grass carp (*Ctenopharyngodon idella*) following challenge with *Aeromonas hydrophila*, a major aquatic pathogen. Six transcriptionally distinct IgM$^+$ B cell subpopulations were identified, including (im)mature B cells, innate B cells, proliferating B cells, IgD^{high} B cells, and two infection-induced subsets denoted as infection Ⅰ and Ⅱ B cells. Bacterial infection altered the cellular heterogeneity of IgM$^+$ B cells, triggered metabolic reprogramming in (im)mature and innate B cell subpopulations, and enhanced the immunological activation of circulating B cells. Notably, infection Ⅰ B cells demonstrated robust induction of interferon φ1 (*IFNφ1*), a type I IFN, following *A. hydrophila* exposure. This induction was further validated through *in vitro* bacterial stimulation, indicating that teleost B cells actively contribute to innate antibacterial responses through IFN signaling. Additionally, the IgD^{high} B cell subpopulation remained consistently present in peripheral blood across both infected and uninfected states, pointing to a constitutive and likely mature phenotype. These findings significantly advance our understanding of the heterogeneity of peripheral blood IgM$^+$ B cells and provide new insights into IgM$^+$ B cell-mediated immune responses in teleost fish.

Keywords: ScRNA-seq; B cells; Peripheral blood; Grass carp; Bacterial infection

INTRODUCTION

In mammals, B cells migrate from central lymphoid organs to peripheral immune sites via the circulatory system, where they differentiate and execute effector functions in response to immunological stimuli, including antibody production and modulation of cellular immunity (Hoffman et al., 2016). These cells comprise a heterogeneous population composed of distinct functional subsets (Bhattacharya, 2018), including naïve B cells, plasma cells, memory B cells, and regulatory B cells, each arising from divergent developmental trajectories (Akkaya et al., 2020; Lebien & Tedder, 2008; Shen & Fillatreau, 2015). B cell phenotype and function are further influenced by pathological conditions, local microenvironment, and aging (Cancro, 2020; Morgan & Tergaonkar, 2022). Although mammalian B cell subpopulations have been extensively characterized, their counterparts in teleost fish—the early jawed vertebrates to exhibit adaptive immune responses—remain incompletely understood, particularly within the peripheral blood compartment.

While five immunoglobulin isotypes (IgM, IgD, IgA, IgG, and IgE) have been described in mammals, only three (IgM, IgD, and IgT) have been identified in teleosts (Sun et al., 2020). Among them, IgM is an evolutionarily conserved isotype found across all jawed vertebrates (Amemiya et al., 2013). In teleosts, IgM$^+$ B cells represent the most abundant B cell population and play a central role in systemic immune

This is an open-access article distributed under the terms of the Creative Commons Attribution Non-Commercial License (http://creativecommons.org/licenses/by-nc/4.0/), which permits unrestricted non-commercial use, distribution, and reproduction in any medium, provided the original work is properly cited.

Copyright ©2025 Editorial Office of Zoological Research, Kunming Institute of Zoology, Chinese Academy of Sciences

Received: 08 March 2025; Accepted: 09 April 2025; Online: 10 April 2025

Foundation items: This work was supported by the National Natural Science Foundation of China (32373162, 31972824), Major Science and Technology Project of Hubei Province (2023BBA001), HZAU-AGIS Cooperation Fund (SZYJY2023006), and China Agriculture Research System of MOF and MARA (CARS-46)

*Corresponding authors, E-mail: yonganzhang@mail.hzau.edu.cn; xujiezhang@mail.hzau.edu.cn

responses (Zhang et al., 2010). Recent advances in single-cell RNA sequencing (scRNA-seq) have enabled detailed characterization of the immune cell landscape in several teleost species, including Mexican tetra (*Astyanax mexicanus*) (Ferrero et al., 2020; Peuß et al., 2020), zebrafish (*Danio rerio*) (Ferrero et al., 2020; Tang et al., 2017), rainbow trout (*Oncorhynchus mykiss*) (Perdiguero et al., 2021), grass carp (*Ctenopharyngodon idella*) (Pan et al., 2023), Nile tilapia (*Oreochromis niloticus*) (Wu et al., 2021), and Atlantic cod (*Gadus morhua*) (Guslund et al., 2020). In rainbow trout, peripheral blood MHCⅡ$^+$ lymphocytes, corresponding to circulating B cells, have been divided into 10 clusters based on differences in functional enrichment pathways (Perdiguero et al., 2021). Our previous work in grass carp revealed six subpopulations in head kidney IgM$^+$ B cells, including (im)mature B cells, innate B cells, proliferating B cells, plasma cells, CD22$^+$ cells, and CD34$^+$ cells (Pan et al., 2023). Additionally, in rainbow trout, clonal expansion and somatic hypermutation of antigen (Ag)-specific IgM$^+$ B cells have been observed within primordially organized germinal center-like structures in the spleen (Shibasaki et al., 2023). Although growing evidence supports the heterogeneity of teleost IgM$^+$ B cells, their tissue-specific distribution and pathogen-responsive dynamics remain largely unresolved.

In addition to their canonical role in antibody production, mammalian B cells perform a range of antibody-independent functions, most notably through the secretion of immunomodulatory cytokines (Lund, 2008). Among the best-characterized cytokine-secreting subsets are B10 cells, which secrete interleukin-10 (IL-10) and suppress CD4$^+$ T cell responses (Lykken et al., 2015). Effector B cell populations in mice include Be1 and Be2 cells, with the former secreting interferon-γ (IFN-γ), tumor necrosis factor-α (TNF-α), and IL-12 and the latter releasing IL-4 and IL-10 (De Gruijter et al., 2022). Pathogen exposure can also trigger B cells to secrete cytokines; for instance, parasitic infection can promote B cell secretion of IL-17 (Hao et al., 2011), while bacterial and viral infection can generate IFN-γ-producing CD11a^{hi}FcγRⅢ^{hi} B cell subpopulations in mice (Bao et al., 2014). In contrast, cytokine-secreting B cells remain poorly characterized in teleosts, although the pronounced innate features of teleost B cells, such as phagocytic activity, have drawn increasing interest. Further investigation is necessary to determine the existence of unidentified teleost B cell subpopulations, particularly cytokine-secreting subpopulations.

In the present study, grass carp were challenged with the pathogenic bacterium *Aeromonas hydrophila*, and peripheral blood IgM$^+$ B cells were profiled using scRNA-seq. A distinct IgD^{high} B cell subpopulation was consistently detected across both infected and uninfected individuals, suggesting a constitutive presence within the circulating IgM$^+$ B cell compartment. Additionally, two infection-inducible IgM$^+$ B cell subpopulations were identified, one promoting innate immune responses via up-regulation of *IFNφ1*, and another marked by elevated *CD9 like* expression. These findings expand our current understanding of teleost B cell heterogeneity and provide new insights into the innate and adaptive features of B cell-mediated immunity in teleost fish.

MATERIALS AND METHODS

Lead contact and materials availability

No unique reagents were generated in this study. Further information and requests for resources and reagents should be directed to and will be fulfilled by the lead contacts (Y.A.Z. and X.J.Z.).

Ethics statement

All animal experiments were approved by the Animal Ethic Committee of Huazhong Agricultural University (HZAUFI-2024-0046), and all efforts were made to minimize the suffering of animals.

Fish and bacterial infection

Healthy grass carp, weighing approximately 150±20 g, were obtained from Huanggang, Hubei Province, China. Fish were maintained in recirculating aquarium systems at the College of Fisheries, Huazhong Agricultural University, under controlled environmental conditions (27–29°C, 12 h light/dark photoperiod). The fish were fed twice daily with commercial diets and acclimatized to laboratory conditions for at least 2 weeks prior to experimentation. No clinical abnormalities were observed during this period.

The *A. hydrophila* strain XS91-4-1 stored in our laboratory was used for bacterial challenge.

Bacterial challenge

Aeromonas hydrophila was prepared as previously described (Pan et al., 2023) and resuspended in sterile phosphate-buffered saline (PBS, Invitrogen, USA) to a final concentration of 7.5×10^6 CFU/mL. Thirty grass carp were randomly distributed into two tanks (15 fish per tank) and intraperitoneally (i.p.) injected with 200 μL of *A. hydrophila* or PBS (control).

Tissue collection

Sixteen days post-infection, peripheral blood leukocytes were collected from five fish per group. Briefly, fish were euthanized using MS-222 (Sigma, USA), and blood was collected from the caudal vein with heparinized needles. Samples were diluted 10 times with Dulbecco's Modified Eagle Medium (DMEM, Life Technologies, USA) supplemented with 100 U/mL penicillin, 100 μg/mL streptomycin, and 25 U/mL heparin (Sigma, USA). Leukocytes were isolated by density gradient centrifugation using 51%/34% discontinuous Percoll (GE Healthcare, USA) as previously described (Zhang et al., 2010), centrifuged at 400 ×*g* for 30 min at 4°C. Leukocytes at the interface were collected, washed twice with DMEM, resuspended in DMEM, and kept on ice until further use.

Cell sorting

Leukocytes were incubated with the mouse anti-grass carp IgM monoclonal antibodies (1 μg/mL; 99-9-A4-A12) in PBS containing 2% fetal bovine serum (FBS, Thermo Fisher Scientific, USA) for 45 min on ice (Cui et al., 2020). After three washes, cells were resuspended in PBS containing 2% FBS (Gibco, New Zealand) and incubated with allophycocyanin-conjugated goat anti-mouse IgG antibodies (2 μg/mL; BioLegend, USA) on ice for 30 min. Following another three washes, cells were resuspended in PBS containing 5 μg/mL propidium iodide (PI; Thermo Fisher Scientific, USA) for 5 min. Live IgM-positive cells were isolated by fluorescence-activated cell sorting (FACS) using MoFlo XDP (Beckman, USA). The gating strategy was applied to exclude cell debris, adherent cells, and dead cells from the sorted IgM$^+$ B cells based on the forward-scatter (FSC)/side-scatter (SSC) profile and fluorescence of PI.

Single-cell library preparation and sequencing

Single-cell transcriptome libraries of the sorted IgM$^+$ B cells

were prepared as described previously (Pan et al., 2023). To minimize inter-individual variation, the sorted IgM$^+$ B cells from five fish in each group were mixed and adjusted to 1 000 cells/μL. Cells from both infected and control groups were processed simultaneously. Chromium Controller with Chromium Single Cell V3 Chemistry Library Kit, Gel Bead & Multiplex Kit, and Chip Kit (10× Genomics, USA) were used. Transcripts were converted to cDNA, barcoded, and libraries were sequenced on the Illumina NovaSeq 6000 platform (Illumina, USA).

ScRNA-seq data processing

Raw sequencing reads in FASTQ format were aligned to the grass carp reference genome using the 10× Genomics Cell Ranger Pipeline (v.8.0.1) under default settings, generating gene-barcode matrices (Wu et al., 2022), with each matrix element representing the number of unique molecular identifiers (UMIs) associated with the gene and barcode. Filtered expression matrices, containing only high-confidence cell-associated barcodes, were subsequently loaded into the Seurat R package (v.4.4.0) for further analysis and visualization (Satija et al., 2015).

Quality control, normalization, and dimensionality reduction

Cells were excluded if mitochondrial gene content exceeded 5% or if hemoglobin subunit gene expression represented more than 5% of total UMIs, to remove damaged cells and erythrocyte contamination. Only cells with UMI counts below 15 000 and between 200 and 2 500 detected genes were retained. Expression matrices from all samples were merged using Seurat and normalized using the "LogNormalization" method. The top 3 000 highly variable genes were identified using the *FindVariableFeatures* function. Expression data for these genes were normalized, scaled, and centered using the *ScaleData* function. Principal component analysis (PCA) was then performed on these genes, and the top 20 principal components were used for integration across samples using the *RunHarmony* function in the Harmony R package (v.1.2.1), corrected for batch effects (Korsunsky et al., 2019). The top 20 dimensions generated by Harmony were used for clustering and tSNE analyses with the *FindNeighbors* and *RunUMAP* functions, respectively.

Cell clustering and annotation

Cell clusters were identified using the *FindClusters* function with a resolution of 0.5. Differentially expressed genes (DEGs) among clusters were determined using the *FindAllMarkers* function with the Wilcoxon Rank-Sum test. Cluster identities were assigned based on canonical marker genes, including interferon regulatory factor 8 (*IRF8*; GenBank accession number: XM_051871037.1), CC motif chemokine ligand 4 (*CCL4*; EU918199.2), interferon regulatory factor 4b (*IRF4b*; XM_051876470.1), immunoglobulin δ 1 (*IgD1*; PQ678980), immunoglobulin δ 2 (*IgD2*; PQ678981), immunoglobulin δ 3 (*IgD3*; PQ678982), programmed cell death 1 ligand 1 (*PD-L1*; XM_051877173.1), DNA topoisomerase 2-a (*TOP2a*; XM_051914803.1), ubiquitin-conjugating enzyme E2C (*UBE2C*; XM_051897767.1), antigen Ki-67 (Ki-67; XM_051914419.1), single-stranded DNA cytosine deaminase (*AICDA*; XM_051864491.1), class of major histocompatibility complex Ⅱα (*MHCⅡα*; EU186148.1), interferon alpha-inducible protein 27-like 2A (*IFI27L2a*; PQ678983), myxovirus resistance 3 (*Mx3*; XM_051890927.1), grass carp reovirus (GCRV)-induced gene 2i (*GIG2i*; PQ678984), interferon-stimulated gene 152 (*ISG152*; KX421263.1), signal transducer and activator of transcription 1 (*STAT1*; KU508677.1), signal peptidase complex catalytic subunit SEC11A (*SEC11A*; XM_051870320.1), signal peptidase complex subunit 3 (*SPCS3*; XM_051907613.1), peptidyl-prolyl cis-trans isomerase B (*PPIB*; XM_051883914.1), peptidyl-prolyl cis-trans isomerase (*PPIs*; XM_051907839.1), and cluster of differentiation 9 like (*CD9 like*; XM_051891113.1). Clusters assigned to the same cell type were merged. Differentially expressed transcripts distinguishing each cell cluster are provided in Supplementary Table S1.

Enrichment analysis

DEGs were identified using the *FindAllMarkers* function in Seurat, with selection criteria set to avg_log2fold-change>0.26303 and p_val_adj<0.05. Functional enrichment analyses, including Gene Ontology (GO) and Kyoto Encyclopedia of Genes and Genomes (KEGG) pathway analyses, were conducted using the OmicShare online platform (http://www.omicshare.com/tools). GO terms and KEGG pathways with P<0.05 were considered significantly enriched.

RNA velocity and pseudotime trajectory analysis

RNA velocity analysis was performed using Velocyto (v.0.17.17) with default parameters to predict the differentiation dynamics of peripheral blood IgM$^+$ B cells from both control and infected grass carp (La Manno et al., 2018). Further analysis and visualization were performed using the Python package scVelo (v.0.3.2) (Bergen et al., 2020).

Pseudotime analysis was carried out with Monocle 2 (v.2.30.1) (Qiu et al., 2017). Genes for unsupervised cell ordering were selected as the union of the top 2 000 highly variable genes across total IgM$^+$ B cells, following Monocle 2 documentation (https://github.com/cole-trapnell-lab/monocle-release). Dimensionality reduction was conducted using the *Discriminative Dimensionality Reduction with Trees* (*DDRTree*) algorithm. Dynamic gene expression was visualized using the *plot_genes_in_pseudotime* function.

Scoring of biological processes

Biological process scores were calculated using the *AddModuleScore* function in Seurat. The aging score was derived from genes annotated under the term aging (GO: 0007568), and the apoptosis score from the apoptosis pathway (GO: 0006915). The oxidative phosphorylation (OXPHOS) score was based on genes associated with oxidative phosphorylation (GO: 0006119). The electron transport chain (ETC) score was calculated using genes related to the electron transport chain (GO: 0022900). The fatty acid metabolism score was calculated using genes related to fatty acid metabolism (GO: 0006631). The glycolytic score was calculated using genes involved in glycolysis (GO: 0006096). The pentose-phosphate score was calculated using genes related to the pentose-phosphate shunt (GO: 0006098). The tricarboxylic acid cycle (TCA) score was calculated using genes associated with the tricarboxylic acid cycle (GO: 0006099).

Cell stimulation

Aeromonas hydrophila was heat-inactivated at 90°C for 30 min and subsequently used as a stimulant. IgM$^+$ B cells, sorted as previously described, were seeded into 24-well plates at a density of 5×10^6 cells/mL and incubated with heat-

inactivated *A. hydrophila* (cell:bacterium=1:10) or with PBS as a control. Cells were incubated at 28°C for different periods of time, depending on the experimental conditions.

Real-time polymerase chain reaction (qPCR) of stimulated cells

Total RNA was isolated from stimulated IgM$^+$ B cells using a HiPure Total RNA Plus Mini Kit (R4121; Magen, China), following the manufacturer's instructions. Reverse transcription was performed using a PrimeScript™ FAST RT reagent Kit with gDNA Eraser (RR092S; Takara, Japan), according to the manufacturer's instructions. Transcript levels of IFNφ1 and related pathway genes were quantified using the CFX96 Connect Real-time System (BioRad, USA) with ChamQ SYBR Color qPCR Master Mix (Q411-02; Vazyme, China). The specific primers used were: β-actin-F, 5' AGC CAT CCT TCT TGG GTA TG 3'; β-actin-R, 5' GGT GGG GCG ATG ATC TTG AT 3'; IFNφ1-F, 5' AAG CAA CGA GTC TTT GAG CCT 3'; IFNφ1-R, 5' GCG TCC TGG AAA TGA CAC CT 3'; TLR3-F, 5' GAG AAC AAT CGT GAC TCC CTG A 3'; TLR3-R, 5' CCA GTA GAG AAC ACA GCG AGG T 3'; TLR7-F, 5' GAG CAT ACA GTT GAG TAA ACG CAC 3'; TLR7-R, 5' TCT CCA AGA ATA TCA GGA CGA TAA 3'; TLR8-F, 5' TCA CAT CGC TTC CAG GTC TC 3'; TLR8-R, 5' ACG GTG AAA TAA TGG GGG TT 3'. Relative expression levels were calculated using the $2^{-\triangle\triangle CT}$ method.

Statistical analysis

Differences in the expression levels of *IFNφ1* and IFN-related pathway molecules were analyzed by one-way analysis of variance (ANOVA) with Dunnett's *post hoc* test using GraphPad Prism (v.7.0). Data are presented as mean±standard deviation (SD). Additional statistical analyses were performed in R using the Wilcoxon test via the "*stat_compare_means*" function in the "ggpubr" package (v.0.6.0).

RESULTS

ScRNA-seq identifies distinct peripheral blood IgM$^+$ B cell subpopulations in different conditions

To comprehensively capture the molecular repertoire of grass carp peripheral blood IgM$^+$ B cells at single-cell resolution, scRNA-seq was conducted using the 10× Genomics platform (Figure 1A; Supplementary Figure S1). A total of 31 959 high-quality cells were analyzed and visualized via Uniform Manifold Approximation and Projection (UMAP), yielding six distinct lineages: (im)mature B cells, innate B cells, IgD^{high} B cells, proliferating B cells, infection Ⅰ B cells, and infection Ⅱ B cells (Figure 1B; Supplementary Table S1). Innate and proliferating B cells were identified based on established marker genes: *IRF8*, *CCL4*, and *IRF4b* for innate B cells, and *Ki-67*, *UBE2C*, *TOP2a*, and *AID* for proliferating B cells (Hu et al., 2024; Pan et al., 2023) (Figure 1C). A novel subpopulation expressing high levels of *Igδs* and *PD-L1* was identified (Lopez-Medina et al., 2015), designated as IgD^{high} B cells (Figure 1C, D). Following bacterial challenge, the proportion of IgD^{high} B cells increased from 4.15% to 6.66% (Figure 1E). Notably, two novel subpopulations, infection Ⅰ and Ⅱ B cells, emerged after infection. Infection Ⅰ B cells were characterized by elevated expression of *MHCⅡα*, *IFI27L2a*, *GIG2i*, *ISG152*, *Mx3*, and *STAT1* (Bénard et al., 2018; Wirz et al., 2022) (Figure 1C, D), while infection Ⅱ B cells predominantly expressed *CD9 like* (Figure 1C, D) (Castro et al., 2015).

Functional characterization of conserved peripheral blood IgM$^+$ B cell subpopulations

The (im)mature, innate, proliferating, and IgD^{high} B cells were present in both control and infected grass carp and were thus defined as conserved subpopulations. Among these, IgD^{high} and proliferating B cells exhibited up-regulation of *TNF-α*, *Myc-2*, and *CD37* expression (Pearson et al., 2001; Van Spriel et al., 2012) (Figure 2A). Additionally, *CD68*, typically considered a macrophage marker, was also detected in these B cells (Figure 2A). This finding aligns with the hypothesis that vertebrate B cells may have evolved from ancient phagocytes. Previous studies have reported that macrophage-expressed gene 1 (*mpeg*) identifies a subpopulation of B cells in zebrafish (Ferrero et al., 2020; Han et al., 2024), supporting a shared lineage between B cells and macrophages in early vertebrates. Innate B cells showed enriched expression of *CD300a* and *CAPG*, genes linked to migratory capacity and innate function (Dabiri et al., 1992; Silva et al., 2011) (Figure 2A). Proliferating B cells exhibited high levels of *PCNA*, *STMN1*, *TPX2*, and *DNTTIP1* (Baik et al., 2007; Repasky et al., 2004; Takase et al., 1995), consistent with active cell cycle progression and potential for clonal expansion and VDJ rearrangement (Figure 2A). GO enrichment analysis revealed that proliferating B cells were enriched in pathways related to "Cell division", "Cell cycle", "Regulation of mitotic cell cycle phase transition", and "DNA replication" (Figure 2B). In contrast, IgD^{high} B cells were enriched in pathways related to "Translation", "Phagocytosis", "Activation of innate immune response", and "Peptide biosynthetic process" (Figure 2B). Analysis of IgM heavy chain gene expression revealed that *Igμ2* was the most abundantly expressed (Figure 2C). Among the subpopulations, expression of *Igμs* was highest in proliferating B cells, followed by IgD^{high} B cells, innate B cells, and (im)mature B cells (Figure 2C). To assess the developmental maturity of the B cell subpopulations, expression patterns of B cell differentiation-associated genes were analyzed (Zwollo, 2011). Proliferating B cells exhibited high expression of *PAX5* and *XBP1* but lacked *Blimp1* expression. Innate B cells showed elevated expression of *Blimp1*, *IRF4a*, and *XBP1*, while IgD^{high} B cells demonstrated low expression of *XBP1*, *IRF4a*, and *Blimp1* (Figure 2D).

Changes in metabolic profiles of conserved IgM$^+$ B cells following bacterial infection

Metabolic activity across conserved IgM$^+$ B cell subpopulations was evaluated under steady-state conditions. Key metabolic pathways assessed included OXPHOS, ETC, fatty acid metabolism, glycolysis, pentose phosphate shunt, and TCA. Results revealed that IgD^{high} and innate B cells displayed elevated aging scores compared to (im)mature and proliferating B cells (Figure 3A), while apoptosis scores remained relatively unchanged across all subpopulations (Figure 3A). Proliferating B cells exhibited the highest levels of OXPHOS and ETC activity, likely reflecting increased energy demands for cell cycle progression (Figure 3A). Notably, IgD^{high} B cells preferentially utilized fatty acid metabolism for energy production rather than glycolysis (Figure 3B). While no significant differences in fatty acid metabolism or glycolysis were observed between proliferating and (im)mature B cells, the pentose phosphate shunt score was markedly increased in proliferating B cells, suggesting enhanced nucleotide biosynthesis and redox regulation (Figure 3B).

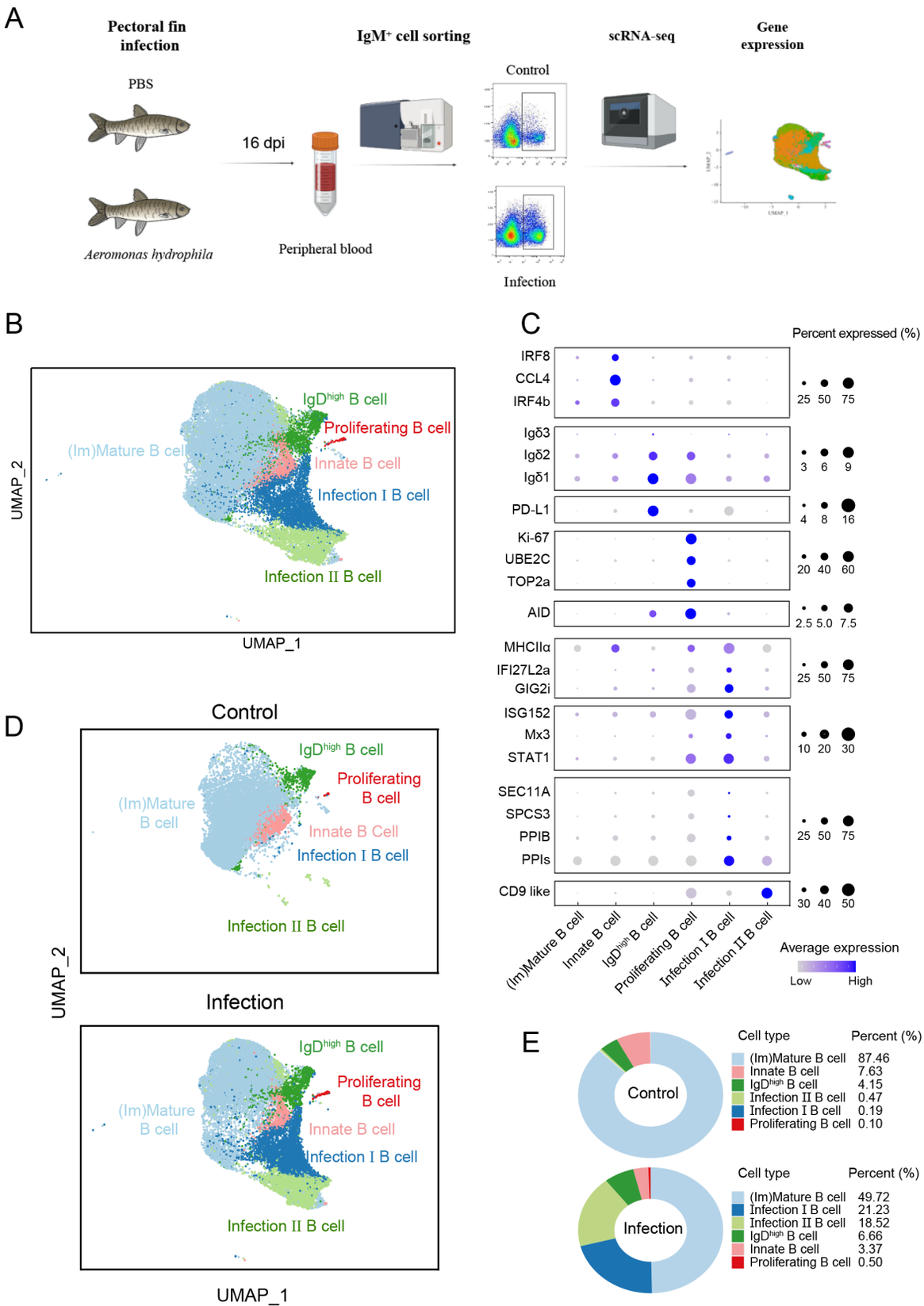

Figure 1 Characterization of grass carp IgM$^+$ B cells in peripheral blood

A: Schematic representation of experimental workflow, including bacterial infection, cell sorting, and scRNA-seq analysis. B: UMAP visualization of 31 959 peripheral blood IgM$^+$ B cells from control (12 034 cells) and infected (19 925 cells) grass carp. Each dot represents a single cell, colored according to cell subpopulation. C: Dot plots depicting expression of selected marker genes in peripheral blood IgM$^+$ B cell subpopulations. D: UMAP visualization of peripheral blood IgM$^+$ B cells from control or infected grass carp. Each dot represents a single cell, colored according to cell subpopulation. E: Proportional representation of each IgM$^+$ B cell subpopulation in control and infected grass carp.

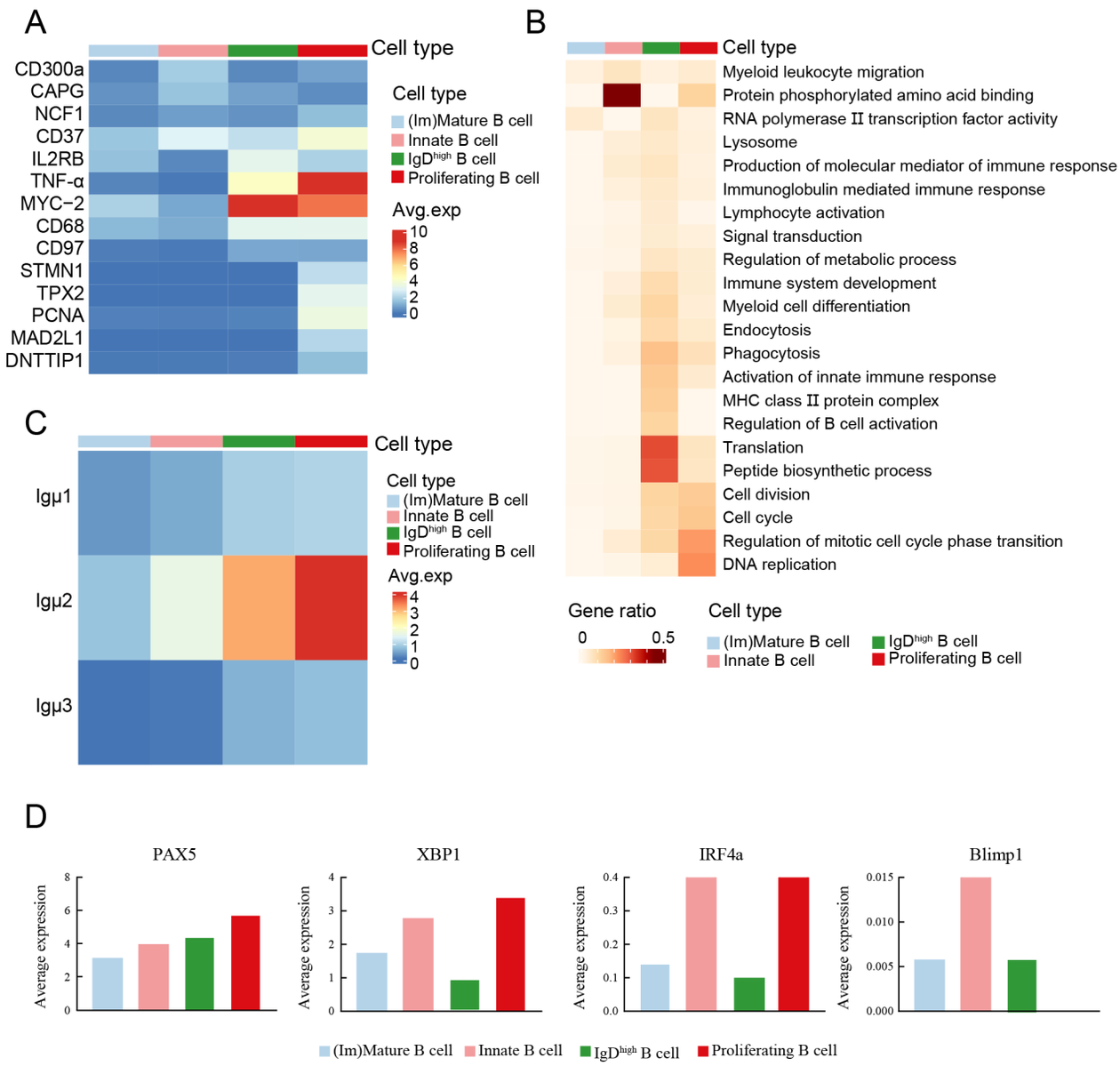

Figure 2 Characterization of IgM⁺ B cell subpopulations in control grass carp

A: Heatmap displaying expression of DEGs in conserved B cell subpopulations. GenBank accession numbers are as follows: CMRF35-like molecule 8 (*CD300a*: XM_051886229.1), macrophage-capping (*CAPG*: XM_051893361.1), neutrophil cytosolic factor 1 (*NCF1*: KX243421.1), cluster of differentiation 37 (*CD37*: XM_051914834.1), interleukin-2 receptor subunit beta (*IL2RB*: XM_051895906.1), tumor necrosis factor-alpha (*TNF-α*: JQ040498.1), transcriptional regulator Myc-2 (*Myc-2*: XM_051897435.1), cluster of differentiation 68 (*CD68*: XM_051898922.1), cluster of differentiation 97 (*CD97*: XM_051885655.1), stathmin (*STMN1*: PQ678985), targeting protein for Xklp2-B (*TPX2*: XM_051880612.1), proliferating cell nuclear antigen (*PCNA*: PQ678986), mitotic spindle assembly checkpoint protein MAD2A like (*MAD2AL1*: XM_051899820.1), deoxynucleotidyl transferase terminal-interacting protein 1 (*DNTTIP1*: XM_051897763.1). Avg.exp represents normalized average expression value of a gene within cell subpopulations. B: Gene Ontology (GO) analysis of DEGs for each subpopulation. GO terms with Benjamini-Hochberg-corrected *P*-values<0.05 (one-sided Fisher's exact test) were selected and colored by gene ratio. C: Heatmap illustrating average expression of each *Igμ* subtype in conserved B cell subpopulations. Avg.exp represents normalized average expression value of a gene within cell subpopulations. D: Bar chart showing average expression of B cell differentiation-related genes in conserved B cell subpopulations. GenBank accession numbers of genes are as follows: paired box 5 (*PAX5*: XM_051888673.1), X-box binding protein 1 (*XBP1*: XM_051894190.1), interferon regulatory factor 4a (*IRF4a*: KU182644.1), B lymphocyte induced maturation protein 1 (*Blimp1*: XM_051866097.1).

Bacterial infection can alter the metabolic state of immune cells (Bantug et al., 2018). Except for proliferating B cells, which maintained stable profiles, the remaining conserved subpopulations showed significant up-regulation of OXPHOS, TCA, and ETC activity following bacterial infection (Figure 3C). Fatty acid metabolism was specifically increased in (im)mature B cells (Figure 3D), while glycolytic activity declined in both (im)mature and innate B cells. Concurrently, the expression of sodium-dependent neutral amino acid transporter-2 (*SNAT2*) was significantly increased, suggesting that glutamine metabolism may play a key role in these two B cell subpopulations following infection (Zwollo, 2011) (Figure 3D).

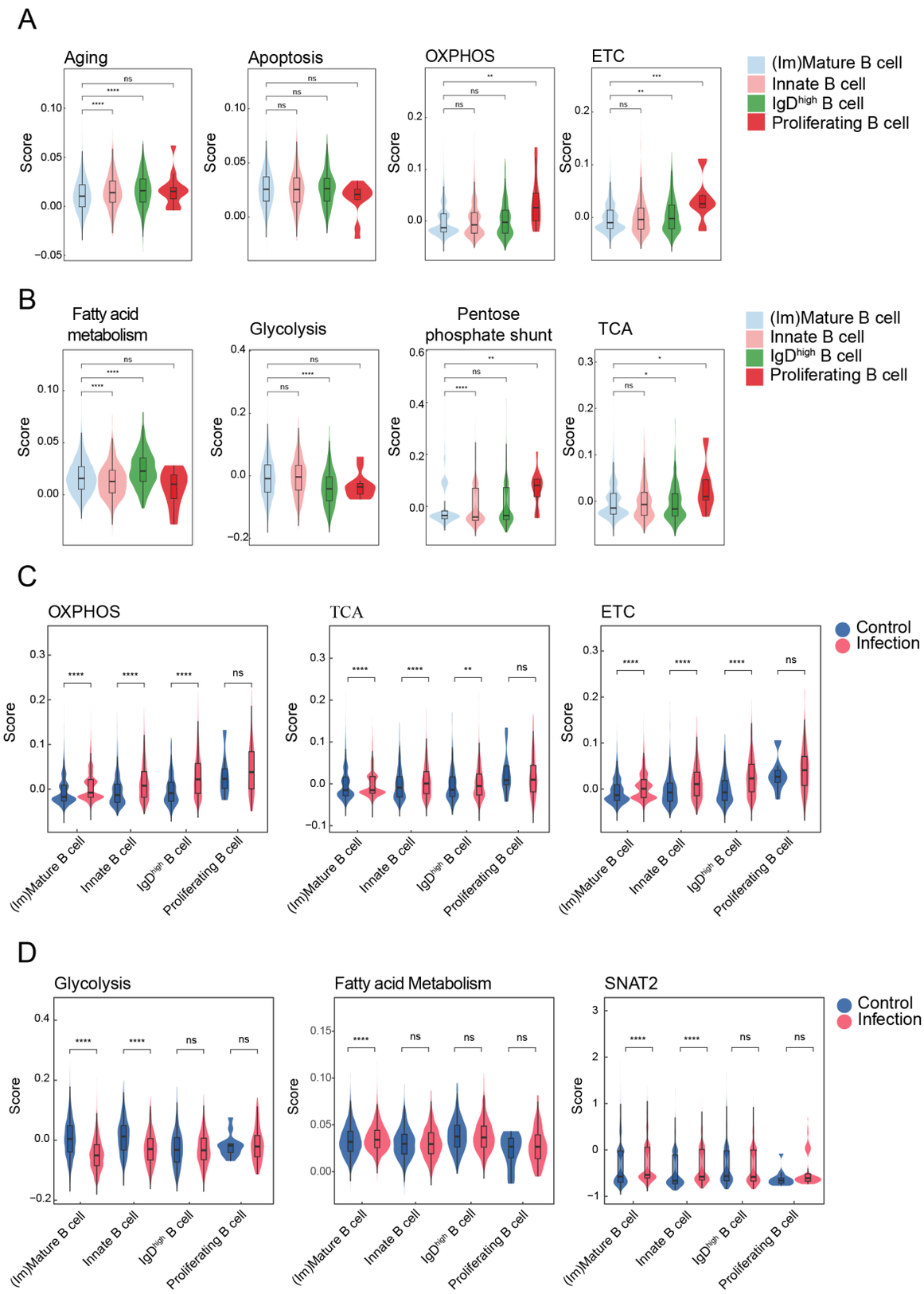

Figure 3 Metabolic process of conserved IgM$^+$ B cell subpopulations

A: Violin plots showing aging, apoptosis, oxidative phosphorylation (OXPHOS), and electron transport chain (ETC) scores for each conserved IgM$^+$ B cell subpopulation. B: Violin plots depicting fatty acid metabolism, glycolysis, pentose phosphate shunt, and tricarboxylic acid (TCA) cycle scores for each conserved IgM$^+$ B cell subpopulation. C: Comparison of OXPHOS, TCA, and ETC scores for each conserved IgM$^+$ B cell subpopulation from control and infected grass carp. D: Comparison of glycolysis, fatty acid metabolism, and sodium-dependent neutral amino acid transporter-2 (*SNAT2*) scores between conserved IgM$^+$ B cell subpopulations from control and infected grass carp. ns: Not significant; *: P<0.05; **: P<0.01; ***: P<0.001; ****: P<0.0001.

Differentiation states of conserved IgM$^+$ B cells following bacterial infection

Bacterial infection did not induce the transcription of immunoglobulin genes in any conserved IgM$^+$ B cell subpopulation (Figure 4A). However, *PAX5* expression was uniformly up-regulated, while *XBP1* and *IRF4a* were down-regulated across all subsets following infection (Figure 4B). The expression levels of *TXNIP*, *SESN1*, *JunB*, and *GADD45B* (Frasca et al., 2019; García-Vega et al., 2024; Shao et al., 2010) as well as *KLF2*, *FOXO3*, *MCL1*, and *CD79b* (Hart et al., 2011; Hinman et al., 2009; Opferman et al., 2003), were up-regulated in all conserved subpopulations upon bacterial infection (Figure 4C). In contrast, the expression levels of *MHCⅡα* and *MHCⅡβ* were down-regulated (Figure 4C). Although phagocytic capacity was improved in (im)mature, IgD^{high}, and innate B cells following bacterial infection, their antigen processing and presentation capabilities were weakened (Figure 4D). To further characterize infection-induced differentiation dynamics, pseudotime trajectories were reconstructed using Monocle, alongside RNA velocity analysis. Result demonstrated a shift in the developmental trajectories of IgM$^+$ B cell subpopulations following infection (Figure 4E). RNA velocity analysis revealed a lack of clear polarized differentiation directions, consistent with Monocle predictions; however, all trajectories converged toward the infection Ⅰ B cell state, indicating a unified transcriptional response to bacterial challenge (Figure 4F).

Characterization of infection-induced IgM$^+$ B cell subpopulations

Infection Ⅰ and Ⅱ B cells, which emerged following infection with *A. hydrophila*, exhibited a greater number of detected genes compared to (im)mature B cells, indicating higher transcriptional activity (Figure 5A). Based on their transcriptional signatures (Figure 1B), infection Ⅰ B cells were defined by robust expression of *IFNφ1*, a gene classically associated with antiviral responses but also implicated in antibacterial defense (Xiao et al., 2021; Zhu et al., 2023). As Toll-like receptors are key sensors of pathogen-associated molecular patterns (e.g., lipopolysaccharides) and are essential for initiating inflammatory responses (Su, 2025), the expression of TLRs and related signaling components was examined. Infection Ⅰ B cells displayed coordinated up-regulation of IFN signaling genes such as *TLRs*, *cGAS*, and *STING* (Erttmann et al., 2022) (Figure 5B). Stimulation of peripheral blood IgM$^+$ B cells with heat-inactivated *A. hydrophila* for 4, 12, and 24 h resulted in significant up-regulation of *IFNφ1* and associated IFN pathway genes (Figure 5C), consistent with the scRNA-seq results. To assess whether these newly emerged subpopulations possess distinct antibody-secreting capacities, the expression of *Igμs* was quantified post-infection. Results showed that *Igμs* expression in the newly emerged subpopulations was similar to that in (im)mature B cells, suggesting that these cells are not differentiating toward plasma cells (Figure 5D). Pseudotime trajectory analysis revealed that both infection I and II B cells predominantly occupied terminal positions along the differentiation axis (Figure 5E).

KEGG pathway enrichment analysis showed that infection Ⅰ B cells were significantly enriched in pattern recognition receptor-related pathways, including “Toll-like receptor signaling pathway”, “RIG-I-like receptor signaling pathway”, “NOD-like receptor signaling pathway”, and “C-type lectin receptor signaling pathway” (Figure 5F), while infection Ⅱ B cells were enriched in “FC gamma R-mediated phagocytosis” and “FoxO signaling pathway” (Figure 5F). Detailed pathway identifiers, expression levels, and statistical significance are provided in Supplementary Table S2.

Co-expression of immunoglobulin genes in peripheral blood IgM$^+$ B cells

The subtypes of grass carp IgM (*Igμ*) and IgD (*Igδ*) heavy chain genes have been described in our previous study (Pan et al., 2023). Here, co-expression patterns of *Igμs* and *Igδs* were examined at the single-cell level in peripheral blood IgM$^+$ B cells from both control and infected grass carp. Among the *Igμ* transcripts, the most frequently observed pattern was *Igμ1*$^-$*Igμ2*$^+$*Igμ3*$^-$, followed by *Igμ1*$^+$*Igμ2*$^-$*Igμ3*$^-$ and *Igμ1*$^+$*Igμ2*$^+$*Igμ3*$^-$ (Figure 6A). Following bacterial infection, the percentage of IgM$^+$ B cells co-expressing *Igμs* increased, with enriched patterns such as *Igμ1*$^+$*Igμ2*$^+$*Igμ3*$^-$, *Igμ1*$^+$*Igμ2*$^-$*Igμ3*$^+$, *Igμ1*$^-$*Igμ2*$^+$*Igμ3*$^+$, and *Igμ1*$^+$*Igμ2*$^+$*Igμ3*$^+$. Co-expression patterns of *Igδs* isoforms were also analyzed. The most common expression pattern in IgM$^+$ B cells was *Igδ1*$^+$*Igδ2*$^-$*Igδ3*$^-$, followed by *Igδ1*$^-$*Igδ2*$^+$*Igδ3*$^-$ (Figure 6B). Notably, in contrast to *Igμs*, co-expression of *Igδs* variants was very low and unaffected by bacterial infection (Figure 6B).

Further analysis of co-expression profiles across individual B cell subpopulations revealed no major infection-induced changes in *Igμs* and *Igδs* co-expression patterns, with the exception of proliferating and IgD^{high} B cells. In the control group, the highest co-expression rate of *Igμs* and *Igδs* in proliferating B cells was 8.33%, with dominant patterns including *Igμ1*$^-$*Igμ2*$^+$*Igμ3*$^-$*Igδ1*$^-$*Igδ2*$^+$*Igδ3*$^-$, *Igμ1*$^+$*Igμ2*$^+$*Igμ3*$^+$ *Igδ1*$^+$*Igδ2*$^-$*Igδ3*$^-$, and *Igμ1*$^+$*Igμ2*$^+$*Igμ3*$^+$*Igδ1*$^+$*Igδ2*$^+$*Igδ3*$^-$ (Figure 6C). Post-infection, this co-expression rate declined to 3.03%, with prevalent configurations such as *Igμ1*$^-$*Igμ2*$^+$ *Igμ3*$^-$*Igδ1*$^+$*Igδ2*$^-$*Igδ3*$^-$, *Igμ1*$^-$*Igμ2*$^+$*Igμ3*$^-$*Igδ1*$^-$*Igδ2*$^+$*Igδ3*$^-$, and *Igμ1*$^+$*Igμ2*$^+$*Igμ3*$^+$*Igδ1*$^+$*Igδ2*$^-$*Igδ3*$^-$ (Figure 6D). A similar reduction in the co-expression rate was observed in IgD^{high} B cells, decreasing from 26.80% to 12.80% after infection (Figure 6C, D).

DISCUSSION

Our earlier work in rainbow trout revealed that B cells represent a substantial fraction of peripheral blood lymphocytes in teleosts, accounting for approximately 57% of circulating lymphocytes (Zhang et al., 2010). This high prevalence underscores the importance of elucidating the heterogeneity of peripheral B cells in these early vertebrates to improve our understanding of immunological roles during homeostasis and infection.

In mammals, peripheral B cells are well recognized as a phenotypically diverse population, exhibiting distinct differentiation and functional states, including IgD$^+$CD27$^-$ naïve B cells, IgD$^-$CD27$^+$ memory B cells, and IgD$^-$CD27^{high} plasmablasts (Kaminski et al., 2012; Meeuwsen et al., 2017; Sanz et al., 2008). While long-lived plasma cells preferentially localize to the bone marrow, memory B cells exhibit tissue-specific distribution and context-dependent expression signatures (Chen & Laidlaw, 2022; Fooksman et al., 2024). However, comparable insight into the tissue-specific heterogeneity of B cells in teleosts remains limited. Our previous single-cell transcriptomic analysis of grass carp head kidney identified six major IgM$^+$ B cell subpopulations: (im)mature B cells, innate B cells, proliferating B cells, plasma

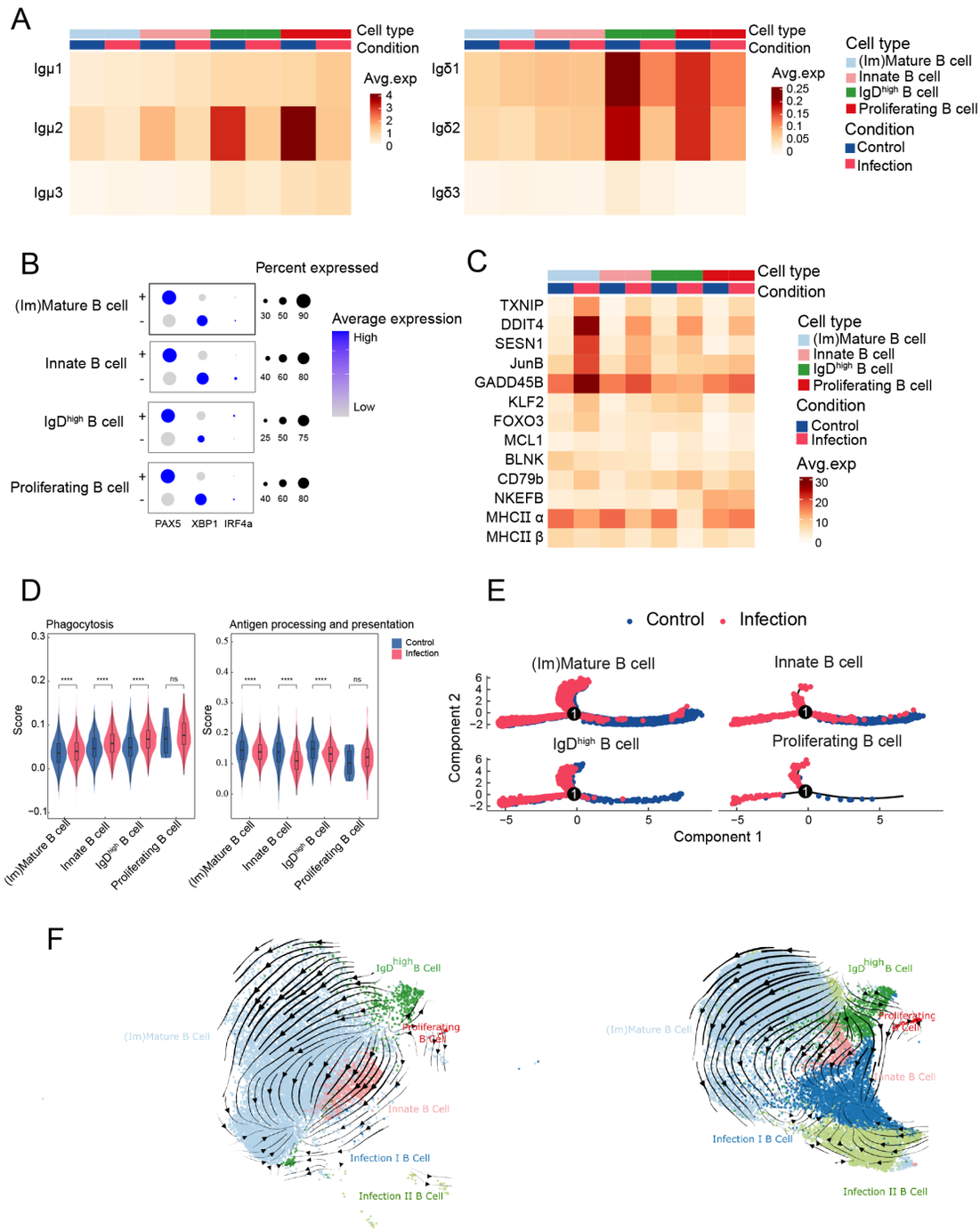

Figure 4 Effects of infection on conserved peripheral blood IgM⁺ B cells

A: Heatmap showing average expression of each *Igμ* (left) and *Igδ* (right) subtype in each conserved IgM⁺ B cell subpopulation. Avg.exp represents normalized average expression value of a gene within cell subpopulations. B: Dot plot showing expression of B cell differentiation-related genes in each conserved IgM⁺ B cell subpopulation before (-) and after (+) *A. hydrophila* challenge. C: Heatmap showing expression of representative genes in each conserved IgM⁺ B cell subpopulation before and after *A. hydrophila* challenge. GenBank accession numbers are as follows: thioredoxin-interacting protein (*TXNIP*: XM_051871792.1), DNA damage-inducible transcript 4 (*DDIT4*: XM_051915381.1), sestrin-1 (*SESN1*: XM_051874404.1) transcription factor Jun-B (*JunB*: DQ298415.1), growth arrest and DNA-damage-inducible beta (*GADD45B*: MH046777.1), Krüppel-like factor 2 (*KLF2*: XM_051910529.1), forkhead box O3B (*FOXO3*: XM_051874162.1), induced myeloid leukemia cell differentiation protein Mcl-1 homolog (*MCL1*: XM_051866610.1), B-cell linker protein-like (*BLNK*: XM_051916847.1), cluster of differentiation 79b (*CD79b*: XM_051915348.1), natural killer-enhancing factor B (*NKEFB*: JX021298.1), class of major histocompatibility complex Ⅱ β (*MHC Ⅱβ*: XM_051904050.1). Avg.exp represents normalized average expression value of a gene within cell subpopulations. D: Violin plots showing phagocytosis, antigen processing, and presentation scores for each conserved IgM⁺ B cell subpopulation. ns: Not significant; *: P<0.05; **: P<0.01; ***: P<0.001; ****: P<0.0001. E: Monocle trajectories of conserved IgM⁺ B cell subpopulations. Each dot represents a single cell. F: Velocity analysis showing inter-relationship of IgM⁺ B cell subpopulations. Velocity fields were projected onto the UMAP plot. Left side represents control group and right side represents infection group.

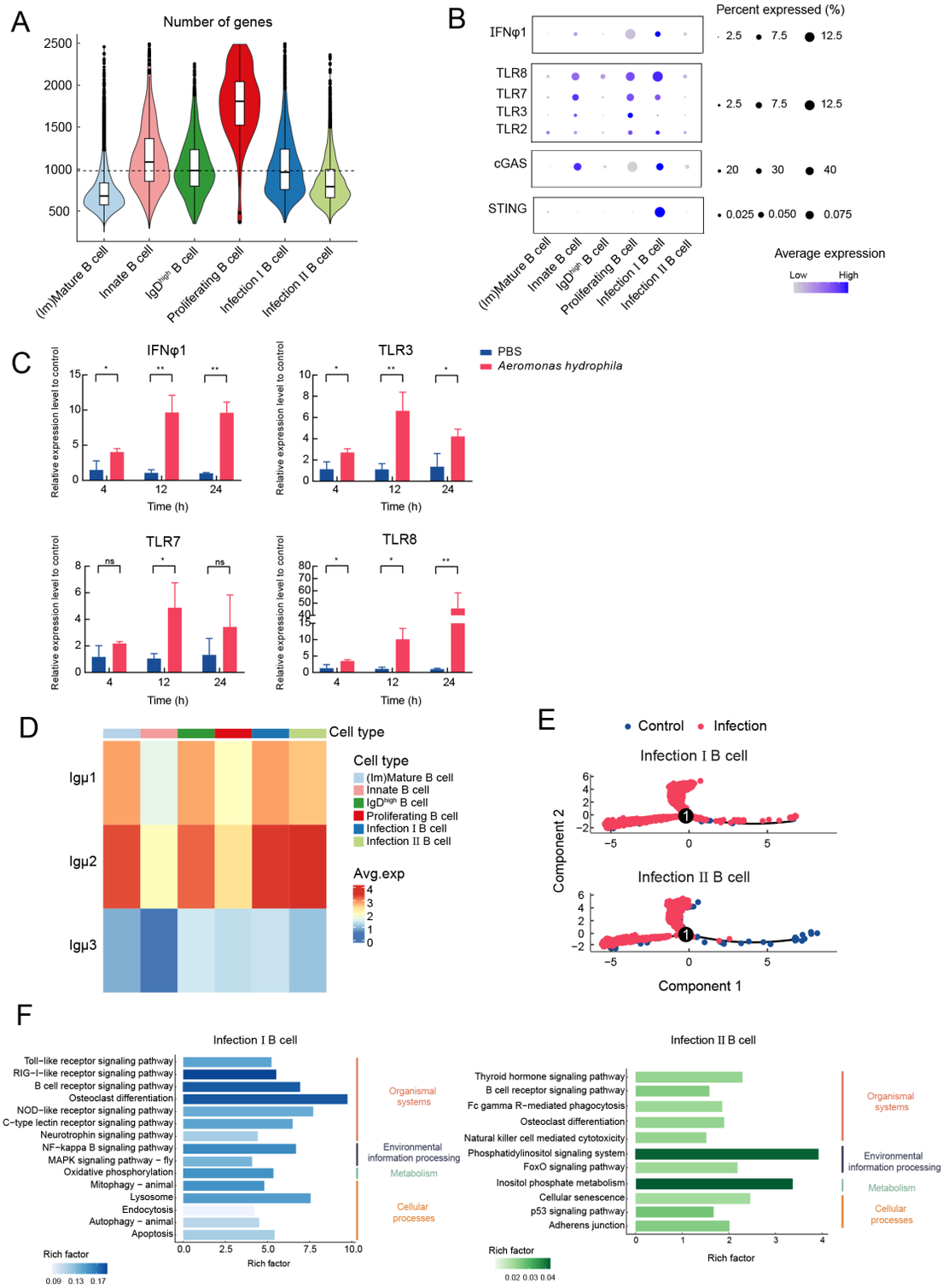

Figure 5 Characterization of newly emerged peripheral blood IgM$^+$ B cell subpopulations following bacterial infection

A: Violin plots showing number of genes expressed in peripheral blood IgM$^+$ B cell subpopulations from infected grass carp. B: Dot plot showing expression of IFN-related genes in peripheral blood IgM$^+$ B cell subpopulations from infected grass carp. GenBank accession numbers are as follows: interferon φ1 (*IFNφ1*: AB180663.1), toll-like receptor 2 (*TLR2*: XM_051918532.1), toll-like receptor 3 (*TLR3*: XM_051893528.1), toll-like receptor 7 (*TLR7*: XM_051904961.1), toll-like receptor 8 (*TLR8*: XM_051904962.1), cyclic GMP-AMP synthase (*cGAS*: XM_051915779.1), stimulator of interferon gene (*STING*: KF494194.1). C: Relative expression of IFN-related genes in peripheral blood IgM$^+$ B cells after *A. hydrophila* stimulation (n=3). Expression (fold change) of IFN-related genes after *A. hydrophila* stimulation was calculated by comparing stimulated cells with control cells using the $2^{-\triangle\triangle Ct}$ method. Data are mean±SD. ns: Not significant; *: P<0.05; **: P<0.01. D: Heatmap showing expression of *Igμ* subclasses in IgM$^+$ B cell subpopulations after *A. hydrophila* challenge. Avg.exp represents normalized average expression value of a gene within cell subpopulations. E: Monocle trajectories of infection Ⅰ and Ⅱ B cells. Each dot represents a single cell. F: KEGG enrichment analysis of DEGs in infection Ⅰ (left) and Ⅱ B cell (right) subpopulations that emerged following infection.

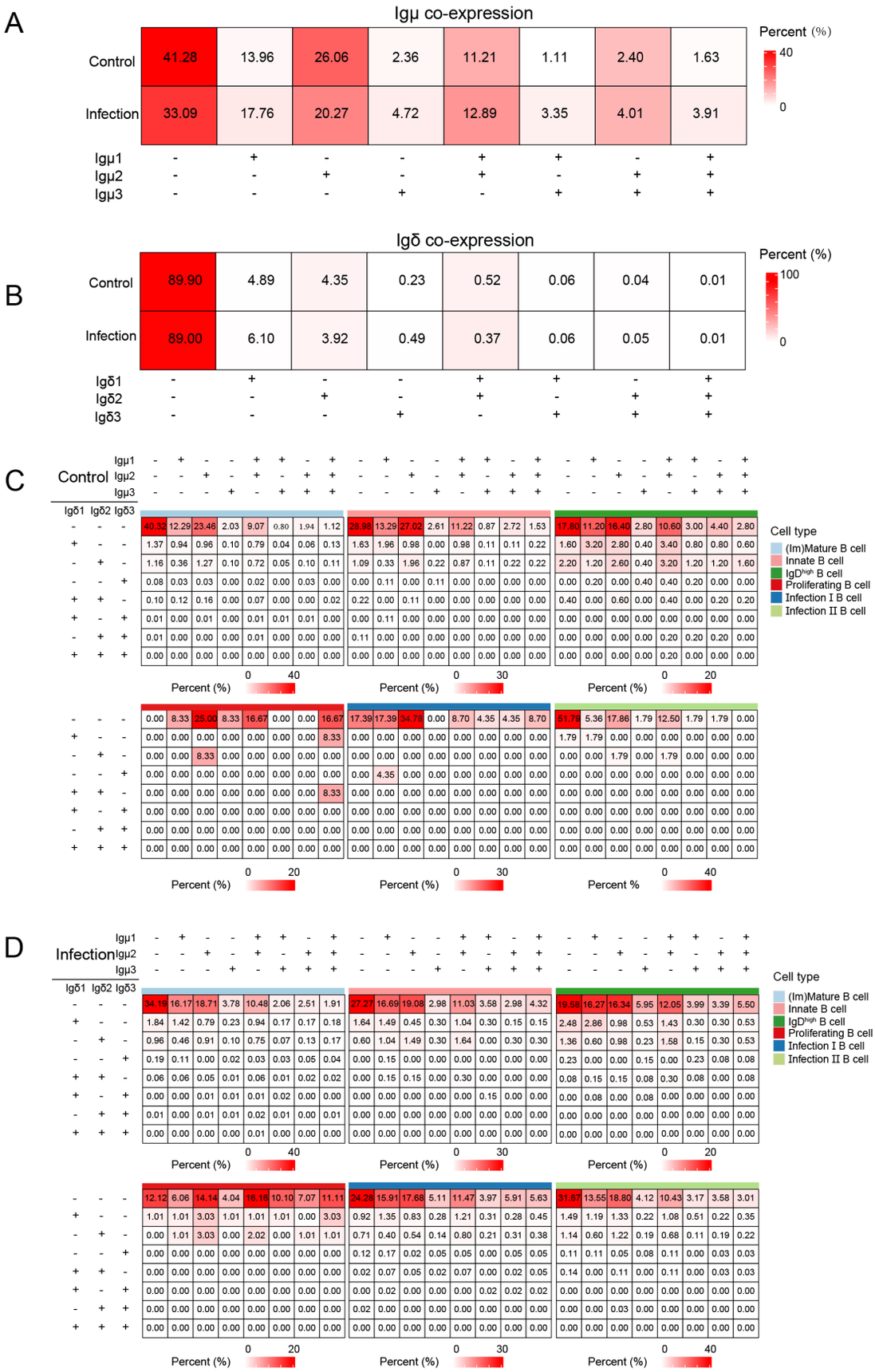

Figure 6 Co-expression of immunoglobulin subclass genes in grass carp peripheral blood IgM$^+$ B cells

A: Heatmap showing percentage of peripheral blood IgM$^+$ B cells expressing *Igμs*. B: Heatmap showing percentage of peripheral blood IgM$^+$ B cells expressing *Igδs*. C: Heatmap showing expression patterns of *Igμs* and *Igδs* in peripheral blood IgM$^+$ B cells from control grass carp. D: Heatmap showing expression patterns of *Igμs* and *Igδs* in peripheral blood IgM$^+$ B cells from infected grass carp. +, positive; −, negative.

cells, CD22$^+$ cells, and CD34$^+$ cells (Pan et al., 2023). To further explore the heterogeneity of peripheral IgM$^+$ B cells and their response to bacterial infection, scRNA-seq was applied to sorted populations from grass carp. Results revealed six major IgM$^+$ B cell subpopulations, including (im)mature, innate, proliferating, IgD^{high}, infection Ⅰ, and infection Ⅱ B cells. Among them, IgD^{high}, infection Ⅰ, and infection Ⅱ B cells were not detected in the head kidney (Pan et al., 2023), indicating compartment-specific divergence of B cell states. These findings suggest that peripheral B cells in teleosts, as in mammals, exhibit microenvironmental heterogeneity and functional diversity, including antibody secretion, cytokine production, and phagocytosis (Abós et al., 2015; Han et al., 2024).

IgD displays significant structural and functional plasticity across vertebrate lineages, largely attributable to variation in the number and composition of Cδ domains (Sun et al., 2020). In teleosts, IgD exhibits greater complexity due to frequent duplication and deletion events involving specific *Cδ* exons. This genomic plasticity has resulted in the emergence of multiple IgD subclasses in species such as channel catfish (*Ictalurus punctatus*), medaka (*Oryzias latipes*), and Atlantic salmon (*Salmo salar*) (Bengtén et al., 2002; Hordvik, 2002; Magadán-Mompó et al., 2011). In mammals, surface expression of IgD-B cell receptor (BCR) is absent on immature B cells, low on transitional B cells, and highest on mature follicular B cells (Avrameas et al., 1979). Similarly, most teleost B cells co-express surface IgM and IgD, with IgD expression typically down-regulated following antigen engagement, reflecting a conserved activation trajectory similar to the behavior of mammalian B cells (Tafalla et al., 2017). We previously identified three *Igδ* genes in the grass carp genome, each encoding different numbers of *Cδ2-Cδ3-Cδ4* domain repeats (Pan et al., 2023). In the current study, three Igδ genes were highly expressed in a distinct IgM$^+$ B cell subpopulation termed IgD^{high} B cells. This subpopulation demonstrated transcriptional enrichment in phagocytosis-related pathways and protein-related genes associated with translation and peptide biosynthesis. IgD^{high} B cells displayed higher *Igμs* expression than (im)mature B cells and a proliferative index second only to proliferating B cells, supporting their classification as mature B cells and suggesting that IgD is preferentially expressed at this stage. Previous studies have reported that peripheral IgM$^+$IgD$^+$ B cells in rainbow trout may represent a mature B cell subset with high antigen-presenting capacity (Perdiguero et al., 2021). Similarly, grass carp IgD^{high} B cells were also enriched in the MHC class Ⅱ protein complex pathway, suggesting a conserved immunological role across teleost species. Notably, a small proportion of plasma cells (Irf4$^+$IgM^{high}IgD^{low}) have been found in the peripheral blood of rainbow trout, comprising only 0.40% of circulating B cells (Perdiguero et al., 2024). In contrast, no transcriptionally defined plasma cell subpopulation was identified in the peripheral IgM$^+$ B cell compartment of grass carp in this study, suggesting that peripheral blood is not a major reservoir for plasma cells in teleosts.

Extensive crosstalk between metabolic reprogramming and B cell fate underscores the importance of nutrient availability and utilization in shaping B cell immune responses (Fu et al., 2022; Jellusova, 2020). Although BCR engagement enhances cellular glucose uptake and glycolytic flux, certain B cell subsets, such as murine germinal center B cells, preferentially rely on fatty acid oxidation for energy (Chen et al., 2021; Weisel et al., 2020). Despite the absence of germinal center-like structures in peripheral blood, grass carp IgD^{high} B cells preferentially utilized fatty acid metabolism relative to other subpopulations. Elevated OXPHOS activity in proliferating B cells suggests a metabolic reliance on the pentose phosphate pathway rather than glycolysis or fatty acid oxidation, consistent with demands for nucleotide biosynthesis and redox regulation (Teslaa et al., 2023). Pathogen-induced metabolic stress is known to drive B cell transformation, as exemplified by Epstein-Barr virus targeting the mitochondrial 1C pathway to support rapid B cell expansion (Rodda & Pepper, 2020; Wang et al., 2019). In the present study, *A. hydrophila* infection markedly increased energy demands in grass carp IgM$^+$ B cells, accompanied by enhanced fatty acid metabolism and up-regulation of *SNAT2* (*SLC38A2*) in specific subpopulations, highlighting fatty acids and amino acids as key metabolic substrates for antibacterial defense. These findings suggest that dietary supplementation with fatty acids and amino acids may augment teleost B-cell mediated anti-infective activity.

In mammals, certain B cell subpopulations contribute to immunoregulation by secreting cytokines; for instance, regulatory B cells secrete anti-inflammatory mediators such as IL-10, IL-35, and transforming growth factor (TGF)-β to suppress inflammation (Rosser & Mauri, 2015). In contrast, cytokine-producing B cell populations in teleosts remain poorly characterized. Notably, this study identified a distinct IgM$^+$ B cell subpopulation in grass carp peripheral blood that expressed *IFNφ1* following bacterial challenge. While type I IFNs (IFN-I) have garnered considerable attention due to their protective role in antiviral immunity, recent studies have demonstrated that they also play a crucial role in host antibacterial immunity (González-Navajas et al., 2012; Monroe et al., 2010). Teleosts possess a diverse repertoire of IFN-I genes, with grass carp encoding four IFN-I isoforms (*IFNφ1–4*), orthologous to those in zebrafish (Liao et al., 2016). Among them, IFNφ1 has demonstrated broad-spectrum bactericidal activity (Xiao et al., 2021; Zhu et al., 2023). The *IFN-I* expressed by the newly identified subpopulation was confirmed to be *IFNφ1*. Similarly, pathogen stimulation in mice leads to the emergence of non-canonical B cell subsets with atypical immune functions, including the production of high levels of IFN-γ, which enhances macrophage activation and initiates innate immune responses (Bao et al., 2014). These findings indicate that the ability of B cells to secrete IFNs in response to infection is evolutionarily conserved from teleosts to mammals, although the specific IFN types produced differ among lineages.

This study provides a comprehensive single-cell characterization of peripheral blood IgM$^+$ B cells in grass carp, revealing substantial heterogeneity in their molecular profiles. Upon bacterial infection, specific IgM$^+$ B cell subpopulations exhibited activation and underwent distinct metabolic reprogramming. Notably, a previously uncharacterized subpopulation capable of secreting IFNφ1 was induced in response to infection. These findings suggest that bacterial vaccination may simultaneously activate both antibody production and IFNφ1-mediated immune responses in teleosts, potentially conferring broad-spectrum immune protection against bacterial and viral pathogens. Validation of this hypothesis will contribute to the development of next-generation vaccines in aquaculture. Collectively, these

findings provide novel insights into the mechanisms by which circulating IgM$^+$ B cells defend against bacterial infections in teleost fish.

DATA AVAILABILITY

The single-cell sequencing data generated in this study have been deposited in the Genome Sequence Archive (GSA) (https://www.scidb.cn/en/c/zoores) under CRA023998, Science Data Bank (doi: 10.57760/sciencedb.j00139.00185), and NCBI (https://www.ncbi.nlm.nih.gov/) under BioProjectID PRJNA1010877.

SUPPLEMENTARY DATA

Supplementary data to this article can be found online.

COMPETING INTERESTS

The authors declare that they have no competing interests.

AUTHORS' CONTRIBUTIONS

Experimental design and conception: X.J.Z., Y.A.Z.; investigation: Y.R.P., X.Q.H., T.T.T.; formal analysis: Y.R.P.; writing-original draft: Y.R.P.; writing-review & editing: X.J.Z., Y.A.Z.; experimental organization and analysis supervision: X.J.Z., Y.A.Z. All authors read and approved the final version of the manuscript.

ACKNOWLEDGMENTS

We thank Yan Wang (Analysis and Testing Center, Institute of Hydrobiology, Chinese Academy of Sciences) for technical assistance in cell sorting.

REFERENCES

Abós B, Castro R, Granja AG, et al. 2015. Early activation of teleost B cells in response to rhabdovirus infection. *Journal of Virology*, **89**(3): 1768–1780.

Akkaya M, Kwak K, Pierce SK. 2020. B cell memory: building two walls of protection against pathogens. *Nature Reviews Immunology*, **20**(4): 229–238.

Amemiya CT, Alföldi J, Lee AP, et al. 2013. The African coelacanth genome provides insights into tetrapod evolution. *Nature*, **496**(7445): 311–316.

Avrameas S, Hösli P, Stanislawski M, et al. 1979. A quantitative study at the single cell level of immunoglobulin antigenic determinants present on the surface of murine B and T lymphocytes. *The Journal of Immunology*, **122**(2): 648–659.

Baik SY, Yun HS, Lee HJ, et al. 2007. Identification of stathmin 1 expression induced by Epstein-Barr virus in human B lymphocytes. *Cell Proliferation*, **40**(2): 268–281.

Bantug GR, Galluzzi L, Kroemer G, et al. 2018. The spectrum of T cell metabolism in health and disease. *Nature Reviews Immunology*, **18**(1): 19–34.

Bao Y, Liu XG, Han CF, et al. 2014. Identification of IFN-γ-producing innate B cells. *Cell Research*, **24**(2): 161–176.

Bénard A, Sakwa I, Schierloh P, et al. 2018. B cells producing type I IFN modulate macrophage polarization in tuberculosis. *American Journal of Respiratory and Critical Care Medicine*, **197**(6): 801–813.

Bengtén E, Quiniou SMA, Stuge TB, et al. 2002. The *IgH* locus of the channel catfish, *Ictalurus punctatus*, contains multiple constant region gene sequences: different genes encode heavy chains of membrane and secreted IgD. *The Journal of Immunology*, **169**(5): 2488–2497.

Bergen V, Lange M, Peidli S, et al. 2020. Generalizing RNA velocity to transient cell states through dynamical modeling. *Nature Biotechnology*, **38**(12): 1408–1414.

Bhattacharya M. 2018. Understanding B lymphocyte development: a long way to go. In: Istifli ES, İla HB. Lymphocytes. IntechOpen.

Cancro MP. 2020. Age-associated B cells. *Annual Review of Immunology*, **38**(1): 315–340.

Castro R, Abós B, González L, et al. 2015. Molecular characterization of CD9 and CD63, two tetraspanin family members expressed in trout B lymphocytes. *Developmental & Comparative Immunology*, **51**(1): 116–125.

Chen CF, Laidlaw BJ. 2022. Chapter one - development and function of tissue-resident memory B cells. *Advances in Immunology*, **155**: 1–38.

Chen DY, Wang Y, Manakkat Vijay GK, et al. 2021. Coupled analysis of transcriptome and BCR mutations reveals role of OXPHOS in affinity maturation. *Nature Immunology*, **22**(7): 904–913.

Cui ZW, Zhang XY, Wu CS, et al. 2020. Membrane IgM$^+$ plasma cells in grass carp (*Ctenopharyngodon idella*): insights into the conserved evolution of IgM$^+$ plasma cells in vertebrates. *Developmental & Comparative Immunology*, **106**: 103613.

Dabiri GA, Young CL, Rosenbloom J, et al. 1992. Molecular cloning of human macrophage capping protein cDNA. A unique member of the gelsolin/villin family expressed primarily in macrophages. *Journal of Biological Chemistry*, **267**(23): 16545–16552.

De Gruijter NM, Jebson B, Rosser EC. 2022. Cytokine production by human B cells: role in health and autoimmune disease. *Clinical and Experimental Immunology*, **210**(3): 253–262.

Erttmann SF, Swacha P, Aung KM, et al. 2022. The gut microbiota prime systemic antiviral immunity via the cGAS-STING-IFN-I axis. *Immunity*, **55**(5): 847–861. e10.

Ferrero G, Gomez E, Lyer S, et al. 2020. The macrophage-expressed gene (*mpeg*) 1 identifies a subpopulation of B cells in the adult zebrafish. *Journal of Leukocyte Biology*, **107**(3): 431–443.

Fooksman DR, Jing ZX, Park R. 2024. New insights into the ontogeny, diversity, maturation and survival of long-lived plasma cells. *Nature Reviews Immunology*, **24**(7): 461–470.

Frasca D, Diaz A, Romero M, et al. 2019. Metabolic requirements of human pro-inflammatory B cells in aging and obesity. *PLoS One*, **14**(7): e0219545.

Fu Y, Wang LM, Yu BC, et al. 2022. Immunometabolism shapes B cell fate and functions. *Immunology*, **166**(4): 444–457.

García-Vega M, Llamas-Covarrubias MA, Loza M, et al. 2024. Single-cell transcriptomic analysis of B cells reveals new insights into atypical memory B cells in COVID-19. *Journal of Medical Virology*, **96**(8): e29851.

González-Navajas JM, Lee J, David M, et al. 2012. Immunomodulatory functions of type I interferons. *Nature Reviews Immunology*, **12**(2): 125–135.

Guslund NC, Solbakken MH, Brieuc MSO, et al. 2020. Single-cell transcriptome profiling of immune cell repertoire of the Atlantic cod which naturally lacks the major histocompatibility class II system. *Frontiers in Immunology*, **11**: 559555.

Han XQ, Cui ZW, Ma ZY, et al. 2024. Phagocytic plasma cells in teleost fish provide insights into the origin and evolution of B cells in vertebrates. *The Journal of Immunology*, **213**(5): 730–742.

Hao Y, O'Neill P, Naradikian MS, et al. 2011. A B-cell subset uniquely responsive to innate stimuli accumulates in aged mice. *Blood*, **118**(5): 1294–1304.

Hart GT, Wang XD, Hogquist KA, et al. 2011. Krüppel-like factor 2 (KLF2) regulates B-cell reactivity, subset differentiation, and trafficking molecule expression. *Proceedings of the National Academy of Sciences of the United States of America*, **108**(2): 716–721.

Hinman RM, Nichols WA, Diaz TM, et al. 2009. *Foxo3-/-* mice demonstrate reduced numbers of pre-B and recirculating B cells but normal splenic B cell sub-population distribution. *International Immunology*, **21**(7): 831–842.

Hoffman W, Lakkis FG, Chalasani G. 2016. B cells, antibodies, and more. *Clinical Journal of the American Society of Nephrology*, **11**(1): 137–154.

Hordvik I. 2002. Identification of a novel immunoglobulin δ transcript and comparative analysis of the genes encoding IgD in Atlantic salmon and Atlantic halibut. *Molecular Immunology*, **39**(1-2): 85–91.

Hu CB, Zhang N, Hong Y, et al. 2024. Single-cell RNA sequencing unveils the hidden powers of zebrafish kidney for generating both hematopoiesis and adaptive antiviral immunity. *eLife*, **13**: RP92424.

Jellusova J. 2020. Metabolic control of B cell immune responses. *Current Opinion in Immunology*, **63**: 21–28.

Kaminski DA, Wei CW, Qian Y, et al. 2012. Advances in human B cell

phenotypic profiling. *Frontiers in Immunology*, **3**: 302.
Korsunsky I, Millard N, Fan J, et al. 2019. Fast, sensitive and accurate integration of single-cell data with Harmony. *Nature Methods*, **16**(12): 1289–1296.
La Manno G, Soldatov R, Zeisel A, et al. 2018. RNA velocity of single cells. *Nature*, **560**(7719): 494–498.
Lebien TW, Tedder TF. 2008. B lymphocytes: how they develop and function. *Blood*, **112**(5): 1570–1580.
Liao ZW, Wan QY, Su JG. 2016. Bioinformatics analysis of organizational and expressional characterizations of the IFNs, IRFs and CRFBs in grass carp *Ctenopharyngodon idella*. *Developmental & Comparative Immunology*, **61**: 97–106.
Lopez-Medina M, Perez-Lopez A, Alpuche-Aranda C, et al. 2015. *Salmonella* induces PD-L1 expression in B cells. *Immunology Letters*, **167**(2): 131–140.
Lund FE. 2008. Cytokine-producing B lymphocytes-key regulators of immunity. *Current Opinion in Immunology*, **20**(3): 332–338.
Lykken JM, Candando KM, Tedder TF. 2015. Regulatory B10 cell development and function. *International Immunology*, **27**(10): 471–477.
Magadán-Mompó S, Sánchez-Espinel C, Gambón-Deza F. 2011. Immunoglobulin heavy chains in medaka (*Oryzias latipes*). *BMC Evolutionary Biology*, **11**(1): 165.
Meeuwsen JAL, van Duijvenvoorde A, Gohar A, et al. 2017. High levels of (un)switched memory B cells are associated with better outcome in patients with advanced atherosclerotic disease. *Journal of the American Heart Association*, **6**(9): e005747.
Monroe KM, McWhirter SM, Vance RE. 2010. Induction of type I interferons by bacteria. *Cellular Microbiology*, **12**(7): 881–890.
Morgan D, Tergaonkar V. 2022. Unraveling B cell trajectories at single cell resolution. *Trends in Immunology*, **43**(3): 210–229.
Opferman JT, Letai A, Beard C, et al. 2003. Development and maintenance of B and T lymphocytes requires antiapoptotic MCL-1. *Nature*, **426**(6967): 671–676.
Pan YR, Wu CS, Zhong YQ, et al. 2023. An atlas of grass carp IgM^+ B cells in homeostasis and bacterial infection helps to reveal the unique heterogeneity of B cells in early vertebrates. *The Journal of Immunology*, **211**(6): 964–980.
Pearson LL, Castle BE, Kehry MR. 2001. CD40-mediated signaling in monocytic cells: up-regulation of tumor necrosis factor receptor-associated factor mRNAs and activation of mitogen-activated protein kinase signaling pathways. *International Immunology*, **13**(3): 273–283.
Perdiguero P, Jiménez-Barrios P, Morel E, et al. 2024. Single-cell atlas of rainbow trout peripheral blood leukocytes and profiling of their early response to infectious pancreatic necrosis virus. *Frontiers in Immunology*, **15**: 1404209.
Perdiguero P, Morel E, Tafalla C. 2021. Diversity of rainbow trout blood B cells revealed by single cell RNA sequencing. *Biology*, **10**(6): 511.
Peuß R, Box AC, Chen SY, et al. 2020. Adaptation to low parasite abundance affects immune investment and immunopathological responses of cavefish. *Nature Ecology & Evolution*, **4**(10): 1416–1430.
Qiu XJ, Mao Q, Tang Y, et al. 2017. Reversed graph embedding resolves complex single-cell trajectories. *Nature Methods*, **14**(10): 979–982.
Repasky JAE, Corbett E, Boboila C, et al. 2004. Mutational analysis of terminal deoxynucleotidyltransferase-mediated N-nucleotide addition in V(D)J recombination. *The Journal of Immunology*, **172**(9): 5478–5488.
Rodda LB, Pepper M. 2020. Metabolic constraints on the B cell response to malaria. *Nature Immunology*, **21**(7): 722–724.
Rosser EC, Mauri C. 2015. Regulatory B cells: origin, phenotype, and function. *Immunity*, **42**(4): 607–612.
Sanz I, Wei CW, Lee FEH, et al. 2008. Phenotypic and functional heterogeneity of human memory B cells. *Seminars in Immunology*, **20**(1): 67–82.
Satija R, Farrell JA, Gennert D, et al. 2015. Spatial reconstruction of single-cell gene expression data. *Nature Biotechnology*, **33**(5): 495–502.
Shao Y, Kim SY, Shin D, et al. 2010. TXNIP regulates germinal center generation by suppressing BCL-6 expression. *Immunology Letters*, **129**(2): 78–84.
Shen P, Fillatreau S. 2015. Antibody-independent functions of B cells: a focus on cytokines. *Nature Reviews Immunology*, **15**(7): 441–451.
Shibasaki Y, Afanasyev S, Fernández-Montero A, et al. 2023. Cold-blooded vertebrates evolved organized germinal center-like structures. *Science Immunology*, **8**(90): eadf1627.
Silva R, Moir S, Kardava L, et al. 2011. CD300a is expressed on human B cells, modulates BCR-mediated signaling, and its expression is down-regulated in HIV infection. *Blood*, **117**(22): 5870–5880.
Su JG. 2025. Toll-like receptor signaling in teleosts. *Science China Life Sciences*, doi: https://doi.org/10.1007/s11427-024-2822-5.
Sun Y, Huang T, Hammarström L, et al. 2020. The immunoglobulins: new insights, implications, and applications. *Annual Review of Animal Biosciences*, **8**(1): 145–169.
Tafalla C, González L, Castro R, et al. 2017. B cell-activating factor regulates different aspects of B cell functionality and is produced by a subset of splenic B cells in teleost fish. *Frontiers in Immunology*, **8**: 295.
Takase K, Terada N, Lucas JJ, et al. 1995. Control of cell cycle entry and progression in mitogen-stimulated human B lymphocytes. *Journal of Cellular Physiology*, **162**(2): 246–255.
Tang Q, Iyer S, Lobbardi R, et al. 2017. Dissecting hematopoietic and renal cell heterogeneity in adult zebrafish at single-cell resolution using RNA sequencing. *Journal of Experimental Medicine*, **214**(10): 2875–2887.
Teslaa T, Ralser M, Fan J, et al. 2023. The pentose phosphate pathway in health and disease. *Nature Metabolism*, **5**(8): 1275–1289.
Van Spriel AB, De Keijzer S, Van Der Schaaf A, et al. 2012. The tetraspanin CD37 orchestrates the $\alpha_4\beta_1$ integrin-Akt signaling axis and supports long-lived plasma cell survival. *Science Signaling*, **5**(250): ra82.
Wang LW, Shen HY, Nobre L, et al. 2019. Epstein-Barr-virus-induced one-carbon metabolism drives B cell transformation. *Cell Metabolism*, **30**(3): 539–555. e11.
Weisel FJ, Mullett SJ, Elsner RA, et al. 2020. Germinal center B cells selectively oxidize fatty acids for energy while conducting minimal glycolysis. *Nature Immunology*, **21**(3): 331–342.
Wirz OF, Jansen K, Satitsuksanoa P, et al. 2022. Experimental rhinovirus infection induces an antiviral response in circulating B cells which is dysregulated in patients with asthma. *Allergy*, **77**(1): 130–142.
Wu CS, Ma ZY, Zheng GD, et al. 2022. Chromosome-level genome assembly of grass carp (*Ctenopharyngodon idella*) provides insights into its genome evolution. *BMC Genomics*, **23**(1): 271.
Wu LT, Gao AL, Li L, et al. 2021. A single-cell transcriptome profiling of anterior kidney leukocytes from nile tilapia (*Oreochromis niloticus*). *Frontiers in Immunology*, **12**: 783196.
Xiao X, Zhu WT, Zhang YQ, et al. 2021. Broad-spectrum robust direct bactericidal activity of fish IFNφ1 reveals an antimicrobial peptide-like function for type I IFNs in vertebrates. *The Journal of Immunology*, **206**(6): 1337–1347.
Zhang YA, Salinas I, Li J, et al. 2010. IgT, a primitive immunoglobulin class specialized in mucosal immunity. *Nature Immunology*, **11**(9): 827–835.
Zhu W, Zhang Y, Liao Z, et al. 2023. IFN1 enhances thrombocyte phagocytosis through IFN receptor complex-JAK/STAT-complement C3.3-CR1 pathway and facilitates antibacterial immune regulation in teleost. *Journal of Immunology*, **210**(8): 1043–1058.
Zwollo P. 2011. Dissecting teleost B cell differentiation using transcription factors. *Developmental & Comparative Immunology*, **35**(9): 898–905.